

Thermodynamic Entropy from Sadi Carnot's Cycle using Gauss' and Doll's-Tensor Molecular Dynamics

William Graham Hoover with Carol Griswold Hoover

Ruby Valley Research Institute

Highway Contract 60, Box 601

Ruby Valley, Nevada 89833

(Dated: February 11, 2022)

Abstract

Carnot's four-part ideal-gas cycle includes both isothermal and adiabatic expansions and compressions. Analyzing this cycle provides the fundamental basis for statistical thermodynamics. We explore the cycle here from a pedagogical view in order to promote understanding of the macroscopic thermodynamic entropy, the state function associated with thermal energy changes. From the alternative microscopic viewpoint the Hamiltonian $\mathcal{H}(q, p)$ is the energy and entropy is the (logarithm of the) phase-space volume Ω associated with a macroscopic state. We apply two novel forms of Hamiltonian mechanics to Carnot's Cycle: [1] Gauss' isokinetic mechanics for the isothermal segments and [2] Doll's Tensor mechanics for the isentropic adiabatic segments. We explore the equivalence of the microscopic and macroscopic views of Carnot's cycle for simple fluids here, beginning with the ideal Knudsen gas and extending the analysis to a prototypical simple fluid.

Keywords: Carnot Cycle, Entropy, Reversible Processes, States, Nonequilibrium Molecular Dynamics

I. FROM PHASE SPACE TO EQUILIBRIUM THERMODYNAMICS

Boltzmann and Gibbs showed that macroscopic thermodynamics, that set of mechanical and thermal relations linking heat, work, temperature, energy, pressure, and volume, is a straightforward consequence of atomistic models of matter. We strengthen that connection here using two relatively recent versions of Hamiltonian mechanics. Gauss' Principle of Least Constraint [applied to the kinetic energy] is the first. It provides a deterministic and time-reversible basis in Hamiltonian mechanics for *isothermal* simulations¹. Doll's Tensor² is the second. It incorporates the macroscopic volumetric strain rate, $(\dot{V}/V) = (\dot{x}/x) + (\dot{y}/y) = 2\dot{\epsilon}$, necessary to simulating mechanical work with *adiabatic* molecular dynamics. These two twentieth-century developments strengthen and illuminate the nineteenth-century connection between microscopic atomistic particle models and macroscopic thermodynamics based instead on empirical constitutive equations of state. Adding the microscopic kinetic-theory notions of ideal-gas thermometry to macroscopic thermodynamic notions of temperature and entropy through Gauss-Principle isothermal and Doll's-Tensor adiabatic deformations provides a straightforward atomistic derivation of macroscopic thermodynamics!

For simple fluids macroscopic equilibrium thermodynamics describes two different kinds of energy changes, dE : [1] heat taken in, dQ , and [2] mechanical work done, dW . For a "reversible" series of equilibrium states the first and second laws of thermodynamics take the form: $dE = dQ - dW = TdS - PdV$. Both energy E and entropy S are equilibrium "state functions" independent of the path taken to reach that state.

Among the concepts connecting the atomistic and thermodynamic descriptions entropy is relatively exotic. Two usual pictures representing entropy are respectively [1] the many-dimensional phase-space volume consistent with a system's longtime trajectory, and [2] the cumulative total of heat divided by temperature on a longtime reversible path from some agreed upon standard state. Unlike energy, pressure, and temperature knowing the detailed microscopic state (coordinates and momenta) is not enough to guess the entropy. The anthropomorphic nature of entropy requires path-dependent details, either past history or future predictions. The simplest route to entropy for a simple fluid begins with Carnot's thought experiment coupling the fluid to an ideal gas constrained to undergo macroscopic changes in temperature and volume.

Accordingly, we describe Carnot's four-part ideal-gas cycle and use that thought experi-

ment construction to define and characterize entropy. This is a traditional textbook path¹. To it we add illustrative microscopic simulations of such cycles for both the ideal gas and an atomistic dense fluid. The simulations use both isothermal and adiabatic extensions of Hamiltonian molecular dynamics. For simplicity we study two-dimensional fluid models, both microscopic and macroscopic, throughout.

The Carnot Cycle itself describes a continuous reversible path of equilibrium states: two expansions and two compressions. The example illustrated in **Figures 1 and 2** is calculated for a two-dimensional monatomic classical ideal gas with the conventional thermal and mechanical equations of state :

$$PV = NkT = E = \sum^N [p_x^2 + p_y^2] / (2m) \quad [\text{Two - Dimensional Ideal Gas}] .$$

The specific equations describing the four-part cycle¹ in the figures shown here connect four sets of (P, V) states:

$$PV = 1; \quad PV^2 = 1; \quad PV = 1/2; \quad PV^2 = 1/2 .$$

Here the Volume V varies from $1/2$ to 2 and back in the following way:

$$(2, 1/2) \xrightarrow{PV=1} (1, 1) \xrightarrow{PV^2=1} (1/4, 2) \xrightarrow{PV=1/2} (1/2, 1) \xrightarrow{PV^2=1/2} (2, 1/2) .$$

These two-dimensional illustrations are adequate and ideally suited to the clarification of mechanical and thermodynamic concepts.

This specific cycle illustrates the state-function nature of entropy S defined by the integral of the heat transfer, weighted with the inverse temperature: $\Delta S \equiv \int dQ/T$. The second and fourth adiabatic parts of Carnot's cycle are free of heat transfer so that we need only consider the first and third in entropy calculations. For an ideal gas there is no potential energy so that these isotherms are also isoenergetic:

$$0 \equiv dE = dQ - dW = TdS - PdV \longrightarrow$$

$$dQ = dW = TdS = PdV = NkT(dV/V) \longrightarrow$$

$$(dQ/T) = dS = Nkd \ln V .$$

The power-law nature of ideal-gas thermodynamics shows that the cyclic integral of dQ/T vanishes for this and any other Carnot Cycle. An arbitrary ideal-gas Carnot cycle can be

subdivided into a grid of infinitesimal isothermal/adiabatic $dP \times dV$ clockwise cycles. Then all the internal cycle integrals cancel their neighbors' contributions. The only exceptions are those perimeter integrals forming the boundary of the larger arbitrary cycle.

Provided that the ideal-gas heat transfers are divided by their temperatures this same conclusion holds for a general fluid matching the thermal heat transfers of the ideal gas. The match is as perfect as is the cycle reversible. Thus the cyclic integrals of (dQ/T) vanish both for the ideal gas and for a general fluid, showing that the entropy S is a state function for both these materials.

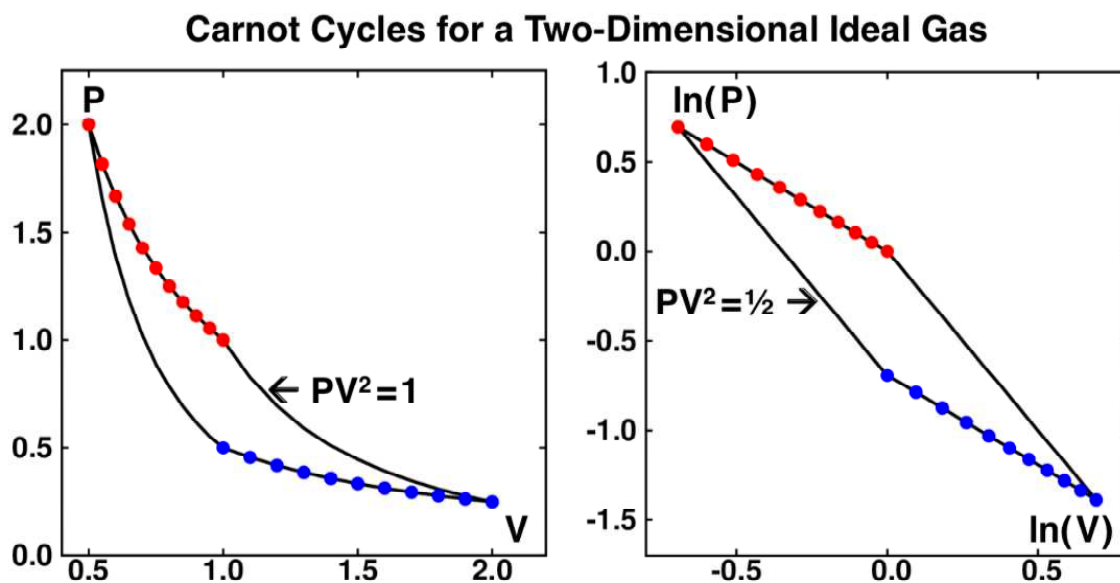


FIG. 1: Sadi Carnot's thermodynamic cycle composed (clockwise from top left) of two twofold expansions, the first isothermal and shown in red, with $T = 1$ and $1/2 < V < 1$. The second expansion, shown black, is adiabatic (no heat transferred) with $1 < V < 2$. The expansions are followed by two twofold compressions, the first isothermal and shown in blue with $T = 1/2$. The second and last adiabatic compression returns the ideal gas to the initial state of the cycle, $(P, V, T) = (2, 1/2, 1)$. The net work done and heat taken in correspond to the area enclosed by the cycle in the left plot. The right plot illustrates the powerlaw forms of the ideal-gas mechanical and thermal equations of state. Notice that the parallel lines show that the isothermal entropy changes, $\pm \ln(V_{\text{hot}}/V_{\text{cold}})$ have equal magnitudes so that $\oint dQ/T$ vanishes. As half of the "hot"-reservoir heat taken in is discharged to the "cold" reservoir at the lower temperature of $(1/2)$, the "efficiency" of this demonstration cycle is "work done"/"heat in" = 50%.

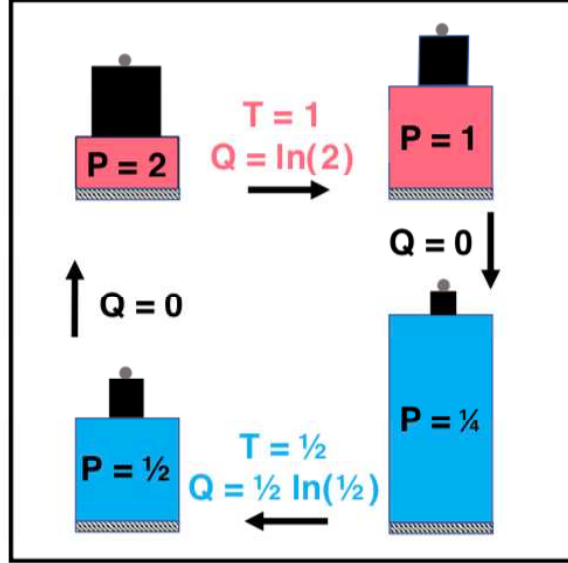


FIG. 2: Sadi Carnot’s thermodynamic cycle connects two “hot” states (at the top, with temperature 1) and two “cold” states (at the bottom, with temperature $1/2$). The vertical adiabatic processes include no heat transfer so that the two isokinetic horizontal processes, with $\Delta Q/T = \pm dS$ give a net entropy change of zero, showing that entropy is a state function. Coupling the isothermal portions of the reversed cycle to a general fluid leads to the same conclusion. So long as the entire cycle is “reversible” the net entropy change vanishes: $\oint dQ/T = 0$. Thus entropy is a state function for a general fluid model.

II. CARNOT CYCLE SIMULATION WITH MOLECULAR DYNAMICS

In March 1980 Hoover, Ladd, Hickman, and Holian described a Doll’s Tensor Hamiltonian incorporating either a shear or a volumetric strain rate conforming to the use of periodic boundary conditions². See the corresponding snapshots in **Figure 3**. The volume strain shown at the left doubles the area. The shear strain at the right imposes a displacement in the x direction varying linearly in y . Volumetric strain is present in all four segments of the Carnot Cycle.² If the four deformations proceed at constant rates notice that the cycle necessarily includes four points where velocity is discontinuous.

The Hamiltonian for the Carnot Cycle problem, has the following form:

$$\mathcal{H}(q, p) = \Phi(q) + K(p) + \dot{\epsilon} \sum_i (x_i p_{x_i} + y_i p_{y_i}) \text{ [Doll's Tensor]} .$$

Here $\dot{\epsilon}$ is the macroscopic strain rate,

$$\dot{\epsilon} = (du_x/dx) = (du_y/dy) = (1/2)(\dot{V}/V) .$$

For simplicity we choose both Boltzmann's constant k and the particle mass m equal to unity throughout. The Doll's Tensor idea is well suited to simulating Carnot's Cycle, both the adiabatic and the isothermal segments. Let us detail the equations of motion.

A. Adiabatic Equations of Motion for Carnot's Cycle

For each of the N particles in a central $L \times L$ periodic cell centered on the origin, $|x|$ and $|y| < (L/2)$, the Doll's Tensor adiabatic equations of motion incorporate the volumetric strain rate $2\dot{\epsilon}$:

$$\{ \dot{x}_i = p_{x_i} + \dot{\epsilon}x_i ; \dot{p}_{x_i} = F_{x_i} - \dot{\epsilon}p_{x_i} , \dot{y}_i = p_{y_i} + \dot{\epsilon}y_i ; \dot{p}_{y_i} = F_{y_i} - \dot{\epsilon}p_{y_i} \} .$$

The isotropic pressure P is given by the Virial Theorem:

$$PV = \sum_i (p_{x_i}^2 + p_{y_i}^2)/2 + \sum_{i<j} (1/2)r_{ij} \cdot F_{ij} ,$$

with

$$r_{ij} = r_i - r_j ; F_{ij} = -\nabla_i \phi(|r_i - r_j|) .$$

The first sum above is over particles and the second is over particle pairs. The Virial Theorem pressure gives the instantaneous rate of energy change:

$$\dot{E} = \dot{\Phi} + \dot{K} \equiv P\dot{V} = -2\dot{\epsilon}PV .$$

These motion equations are ideally suited to the adiabatic deformations in Carnot's cycle, with $\dot{\epsilon}$ positive for the two expansions and negative for the subsequent compressions. The isothermal constraint could be added by the smooth thermostating provided by Nosé-Hoover mechanics³ or by velocity scaling at the end of each timestep:

$$\{ \dot{p}_{x_i} = F_{x_i} - \zeta p_{x_i} ; \dot{p}_{y_i} = F_{y_i} - \zeta p_{y_i} ; \dot{\zeta} = [(K/N) - T]/\tau^2 \} .$$

Trials, with orders of magnitude variation in the Nosé-Hoover relaxation time τ , weren't particularly "useful", in terms of reducing the fluctuations in pressure and temperature in the

course of the cycle. Instead, we successfully used both “Gaussian Mechanics”⁴ and velocity rescaling. Both these algorithms make temperature a constant of the motion. With that choice a 576-particle system with 2304 motion equations is a convenient size for numerical work. We discuss computational applications of the underlying motion equations in the following Sections.

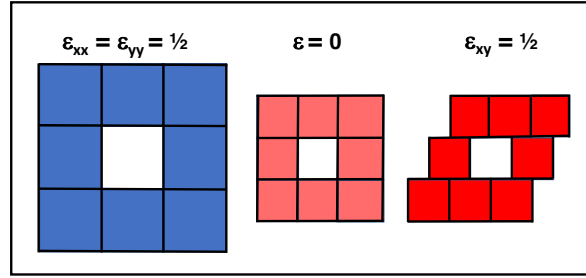


FIG. 3: The central square, with $|x| < L/2$ and $|y| < L/2$ is shown in white. The initial configuration, in the middle, is surrounded by eight periodic images. Expansion, which typically leads to cooling, is indicated at the left and shear, which leads to minor heating, is shown to the right. These boundary conditions lead naturally to the nearest-image convention for computing the forces: $\text{if}(x_{ij} < -L/2) \ x_{ij} = x_{ij} + L$; $\text{if}(x_{ij} > +L/2) \ x_{ij} = x_{ij} - L$. The Carnot cycle of **Figure 1** is composed entirely of volumetric strains, with $\epsilon_{xx} = \epsilon_{yy}$.

B. Isothermal Equations of Motion for Carnot’s Cycle

Adding instantaneous control of the kinetic energy $\sum(p_x^2 + p_y^2)/2$ augments the adiabatic motion equations to include the friction coefficient ζ :

$$\{ \dot{x}_i = p_{x_i} + \dot{\epsilon}x_i ; \dot{p}_{x_i} = F_{x_i} - \dot{\epsilon}p_{x_i} - \zeta p_x , \dot{y}_i = p_{y_i} + \dot{\epsilon}y_i ; \dot{p}_{y_i} = F_{y_i} - \dot{\epsilon}p_{y_i} - \zeta p_y \} .$$

Multiplying the motion equations to compute the kinetic energy K constraint, $\sum(p_x \dot{p}_x + p_y \dot{p}_y) \equiv 0$ provides an explicit equation for the friction coefficient and the resultant motion

equations for the isothermal segments of the cycle:

$$\zeta = \sum_i F_i \cdot p_i / (2K) ; \{ \dot{q} = p + \dot{\epsilon}q ; \dot{p} = F - \zeta p \} .$$

Numerical exploration of the adiabatic and isothermal motion equations shows that both approaches are well-behaved, stable, and relatively close to our expectations based on the thought-experiment version of the Carnot cycle. A useful modification of the isothermal motion equations instead adds a velocity rescaling operation, $p_i \rightarrow p_i \times \sqrt{2NT / \sum p^2}$, at the conclusion of each adiabatic timestep. Accumulating the kinetic energy changes due to these rescalings provides the computational version of heat gain or loss dQ . These energy increments are necessary in evaluating the efficiency and the dissipation associated with the cycles. We describe our computational experience with the Carnot-Cycle molecular dynamics next.

III. COMPUTATIONAL CARNOT CYCLES FOR A KNUDSEN GAS

A practical approach to the nonequilibrium molecular dynamics of the Carnot Cycle is to begin with a conventional four-body computer program incorporating static periodic boundary conditions. Once that isoenergetic programming is successful it is straightforward to introduce dynamic boundaries and to extend Knudsen-gas and dense-fluid codes to larger systems for which fluctuations are smaller. We chose $N = 24^2 = 576$ to illustrate the present work, large enough that the fluctuations are small, but with the system still small enough that laptop problems can be completed in a few hours' time. Equilibrium simulations with zero strain rate suggested a fourth-order Runge-Kutta timestep $dt = 0.001$ with kinetic temperatures of 0.5 and 1.0 for the "cold" and "hot" isothermal segments of the cycle. The minimum and maximum densities imposed on the cycles were $(1/2)$ and (2) , matching our 1991 textbook example problem¹.

Figure 4 shows two views of a (collisionless) Knudsen-Gas cycle. The lack of collisions would seem to suggest, wrongly, that the initial velocity distribution remains unchanged. The adiabatic coordinate changes are paired with momentum changes keeping the phase volume $dqdp$ fixed. The twofold density increases and decreases correspond to twofold increases and decreases in temperature. In the isothermal segments the coordinates expand or contract but the momenta are unchanged. For isothermal processes the kinetic temperature $\langle p_x^2 \rangle = \langle p_y^2 \rangle$ is constant, imposed with the reversible friction ζ or by velocity rescaling. The discontinuous velocities when the four segments begin and end cause no particular computational difficulties.

For the adiabatic segments the Knudsen gas equations of motion,

$$\{ \dot{q} = p + \dot{\epsilon}q ; \dot{p} = -\dot{\epsilon}p \} ,$$

can be integrated analytically (though Runge-Kutta integration is both faster and simpler). Each of the Knudsen-gas momenta varies exponentially in time in the adiabatic segments:

$$p(t) = p(0)e^{-\dot{\epsilon}t} = p(0)e^{-\epsilon} ,$$

where ϵ is the strain and $\dot{\epsilon}$ is the strain rate, for simplicity chosen constant for each segment of the cycle. In the second segment of the cycle, the adiabatic expansion phase, the volume is doubled and the final one-dimensional strain is $\sqrt{2}$. During the expansion the x and y

components of each velocity are reduced by the same factor. The initial Gaussian, with kinetic temperature $\langle p_x^2 \rangle = \langle p_y^2 \rangle = 1$, is reduced in amplitude. This results in the final cooler kinetic temperature $\langle p_x^2 \rangle = \langle p_y^2 \rangle = (1/2)$. The collisionless molecular dynamics reproduces the thought-experiment cycle of **Figure 1** nearly perfectly, as is shown in **Figure 4**.

Analysis of the cycle shows that half the heat taken in at $T = 1$ is given to the cold reservoir at $T = (1/2)$ with the other half converted to work. Each clockwise thermodynamic cycle performs net work equal to $\ln(\sqrt{2})$ per particle.

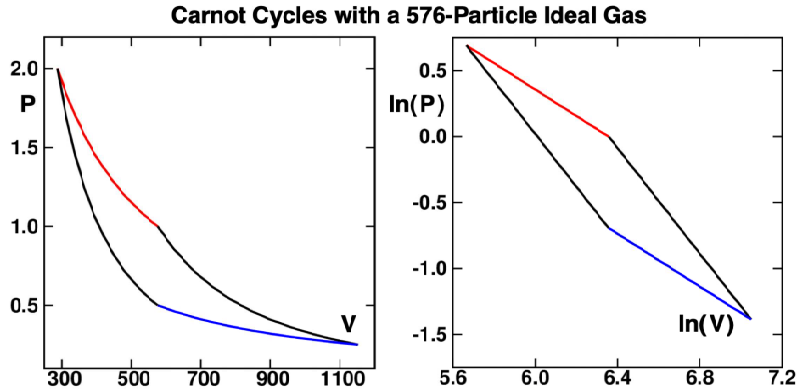


FIG. 4: Knudsen Gas Carnot Cycle with 576 ideal-gas particles. The initial distribution of momenta, chosen Gaussian, remains Gaussian throughout as the temperature varies from 0.5 to 1.0. The four segments of the cycle all correspond to twofold changes in density. The heat taken in at $T = 1$, $\int_{1/2}^1 d \ln V$, $\ln(2)$ per particle, is twice that given off at $T = (1/2)$, with the difference equal to the work done, $288 \times \ln(2)/2 = 199.6$, corresponding with the thought experiment of the theoretical cycle of **Figure 1**.

IV. SIMULATING CARNOT CYCLES FOR A SOFT-DISK DENSE FLUID

For a “realistic” dense-fluid model we use a simple purely-repulsive pair potential with a finite range of unity: $\phi(r < 1) = (10/\pi)(1 - r)^3 \longrightarrow \int_0^1 2\pi r \phi(r) \equiv 1$. Steady-shear simulations with a similar short-ranged repulsive potential, $100(1 - r^2)^4$ suggest that size and strain rate dependences act to reduce the magnitude of the shear viscosity by no more than a few percent⁵. Because Carnot-cycle deformations are volumetric, at constant shape, dissipation occurs in the form of “bulk viscosity” rather than shear. In 1971 David Gass estimated the bulk viscosity for hard disks⁶. Setting the soft-disk potential equal to a kinetic temperature of unity gives an effective diameter of $1 - \sqrt[3]{(\pi/10)} = 0.3202$ from which Gass’ bulk viscosity is roughly 0.04.

We choose the same temperatures, 1 and (1/2), and the same density range, $(1/2) < \rho = (N/V) < 2$ as in the Knudsen Gas example. **Figure 5** shows the resulting cycles for times of 1, 2, 4, and 8 for each of the four segments. Segment times of 256 or 512 are reasonable problems taking only a few hours of laptop time. The longer slower problems show much smaller pressure fluctuations than the faster problems of **Figure 5**. The initial value, PV/N near 1.8, necessarily exceeds the ideal-gas value of unity. Likewise, the minimum, around 0.6, exceeds the ideal-gas value $T = (1/2)$.

The larger slower problems are suitable for thermodynamic analyses of fluctuations. The isokinetic friction coefficient, equivalent to the velocity rescaling factor:

$$\zeta = \frac{\sum_i F_i \cdot p_i}{\sum_i p_i^2}$$

describes the entropy change in thermostatted flows and exhibits large fluctuations in small systems with rapid deformation. We experimented with dozens of combinations of strain rate, timestep, system size and numbers of cycles. A useful estimate of finite-system effects can be based on the series of strain rates $\dot{\epsilon} = (1/2)^n$. Hydrodynamics suggests an entropy production varying as the square of the strain rate, so that for a fixed number of cycles the efficiency should show a loss proportional to the strain rate.

For the series $n = 1$ to 5 we found efficiencies increasing from 88% to 98% of the ideal. In the latter case the lost work per cycle, about 5, should be of order $32(2/32)^2 N\eta_V$, corresponding to a bulk viscosity of order 0.05, close to the hard-disk estimate based on Gass’ work. In all, the agreement of the simulations with expectations is quite satisfactory. The

unaesthetic nature of the velocity discontinuities can only be avoided by adding complexity to the analysis, already clouded by the relatively wide difference in the strain rates.

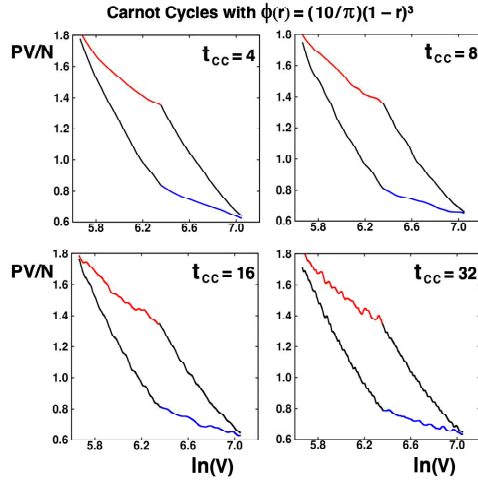


FIG. 5: Soft-disk Carnot Cycle with 576 particles. The pair potential is $\phi(r) = (10/\pi)(1-r)^3$. In the cycle $0.5 < T < 1$ and $(1/2) < \rho < 2$. The work per particle done in the cycle is the enclosed area, roughly 0.4. The total work, larger by a factor of $N = 576$, increases from about 200 to 234 as the cycle time t_{CC} is increased from 4 to 128. The efficiency of the slowest cycle, with $t_{CC} = 512$, is 98% of the ideal 50%.

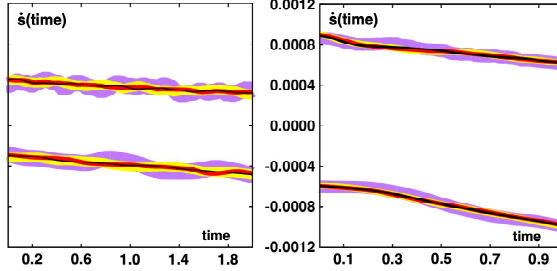


FIG. 6: Entropy gained and lost, by “hot” and “cold” reservoirs respectively in following the dense-fluid Carnot Cycle with periods of 4 (on the right) and 8 (on the left). The numbers of cycles in the averaging vary from 50 to 1000 (left) or 100 to 2000 (right) with the shorter runs (purple) exhibiting larger fluctuations than the longer ones (black). Precise averages require on the order of 100 cycles for 576 particles. The entropy lost by the hot reservoir exceeds that gained by the cold one. The efficiencies of the cycles vary from 88% of the reversible ideal, for the shortest run, to 98% for the longest. Simulations with $dt = 0.01$ are consistent with the $dt = 0.001$ used here.

V. SUMMARY

In Gibbs’ and Boltzmann’s microscopic statistical mechanics entropy is related to the longtime occupation of states in phase space, $S(N, E, V) = k \ln \Omega$. In macroscopic thermodynamics entropy is related to the longtime integrated, slow and reversible, uptake of heat divided by temperature, $S(N, E, V) = \int_{-\infty}^t dQ/T$. Here we have explored these two very different views of entropy for two material models, a Knudsen gas, with a collisionless Maxwell-Boltzmann velocity distribution, and a simple fluid, with a short-ranged purely-repulsive atomistic pair force. We have introduced and used two different versions of nonequilibrium molecular dynamics to implement Carnot Cycles for the two microscopic models.

The Carnot Cycle is fundamental to the connection of phase volume Ω to integrated heat Q and the kinetic temperature T . The cyclic conversion of heat to work cleanly separates macroscopic isothermal and adiabatic volume changes in an elegant way applicable to general fluid models. This cyclic connection of ideal-gas states to fluid states through work and heat provides the simplest possible illustration connecting the microscopic and macroscopic definitions of entropy.

The Carnot Cycle is perfectly suited to two relatively new versions of mechanics: [1] an isothermal mechanics based on Gauss’ Principle of Least Constraint, where the kinetic

temperature is a constrained variable; and [2] an adiabatic mechanics, based on the Doll's-Tensor Hamiltonian,

$$\mathcal{H}_{\text{Doll's}}(q, p) = \mathcal{H}_{\text{Equilibrium}}(q, p) + \dot{\epsilon} \sum_i q_i p_i \rightarrow \dot{E} = -P\dot{V} .$$

This Hamiltonian introduces adiabatic time-dependence into the conservation of mechanical energy, $dE/dt = -PdV/dt = -2\dot{\epsilon}PV$ through the macroscopic strain rate $\dot{\epsilon}$.

Our implementation of the ideal-gas and simple-fluid cycles illustrates the connection of atomistic dynamics to macroscopic thermodynamics. We characterized the dissipative heat for a series of strain rates and related it to bulk viscosity estimates from kinetic theory.

The Carnot cycle is an ideal teaching tool for relating thermodynamics to statistical mechanics. The models suggest further research opportunities. In particular it is desirable to formulate cycles with continuous strainrates and to further detail the microscopic bulk-viscosity mechanism underlying these illustrations of the Second Law of Thermodynamics.

VI. ACKNOWLEDGMENT

We thank Karl Travis and Ed Smith for their cogent comments and suggestions.

- ¹ W. G. Hoover *Computational Statistical Mechanics* (Elsevier, New York, 1991), Section 1.9 “Gauss’ Principle and Nonholonomic Constraints” and Section 2.5 “Second Law of Thermodynamics”. The latter Section details the Carnot Cycle from the macroscopic viewpoint.
- ² W. G. Hoover, A. J. C. Ladd, R. B. Hickman, and B. L. Holian, “Bulk Viscosity *via* Nonequilibrium and Equilibrium Molecular Dynamics”, *Physical Review A* **21**, 1756-1760 (1980).
- ³ H. A. Posch, W. G. Hoover, and F. J. Vesely, “Canonical Dynamics of the Nosé Oscillator: Stability, Order, and Chaos”, *Physical Review A* **33**, 4253-4265 (1986).
- ⁴ D. J. Evans, W. G. Hoover, B. H. Failor, B. Moran, and A. J. C. Ladd, “Nonequilibrium Molecular Dynamics *via* Gauss’ Principle of Least Constraint”, *Physical Review A* **28**, 1016-1021 (1983).
- ⁵ W. G. Hoover and H. A. Posch, “Shear Viscosity *via* Global Control of Spatiotemporal Chaos in Two-Dimensional isoenergetic Dense Fluids”, *Physical Review E* **51**, 273-279 (1995).
- ⁶ D. M. Gass, “Enskog Theory for a Rigid Disk Fluid”, *The Journal of Chemical Physics* **54**, 1898-1902 (1971).